Pyridine Derivatives as Corrosion Inhibitors for Dissolution of Iron Electrode in Tartaric Acid

M. Abdallah, H.E. Megahed and A.M. Atia

Chemistry Department, Faculty of Science, Benha University, BENHA, EGYPT

The corrosion behaviour of iron electrode in de-aerated tartaric acid solutions of varying concentraton (10^{-6} - 1 M) was studied. It was found that, the corrosion potential of Fe varied with acid concentrations while the corrosion rate increased. Addition of some pyridine derivatives on Fe in 10^{-3} M tartaric acid caused a positive shift of steady state potential of iron and the corrosion rate decreased. The potential shift and the inhibition efficiency were found to increase with increasing inhibitor concentration. This led to increase the chemisorption of the inhibitor on the metal surface with the formation of a metal nitrogen co-ordination bond.

A study of corrosion behaviour of iron and steel in mineral acids shows that the corrosion rate increases in the order: $H_3PO_4 < H_2SO_4 < HCl < HNO_3$ [1]. In the first three cases; the corrosion rate increases with increase in acid concentration. However, in concentrated HNO_3, corrosion decreases [2]. Gouda *et. al.* [3] studied the corrosion behaviour of steel in stagnant, deaerated citric and oxalic acid solutions (10^{-5} - 10^{-1} M) in pH range 2-6 and concluded that the corrosion behaviour of steel in dilute organic acid solutions (pH range 2-3) is similar to that obtained in neutral solutions. The corrosion process in these solutions is dependent on the breakdown of the pre-immersion oxide film.

The adsorption of pyridine derivatives on the metallic surface may be expected because of their aromatic nature and the presence of nitrogen (hetero atom). Picolines were used as corrosion inhibitors for the dissolution of Al alloys in HCl [4] and the inhibitive effect was found to increase with increasing the concentration of these compounds.

Phenyl phthalimide derivatives were previously used as corrosion inhibitors for dissolution of iron in oxalic acid [5]. The inhibition efficiency of these derivatives was found to increase with increasing the electronegativity of the substituent. Also, ethoxylated fatty acids [6] and ethoxylated fatty amines [7,8] were used as corrosion inhibitors for iron and C-steel in acidic media.

In industrial processes, tartaric acid is extensively used as neutralizer after cleaning and leaching in the fiber industry. In the present study, an attempt has been made to study potential-time curves for iron electrode.

© E.C.S.I. Bangalore

Polarization measurements were obtained in deaerated solutions of tartaric acid and the effect of the following four derivatives of pyridine on the corrosion of iron in 1 x 10^{-3} M tartaric acid was examined.

Compound I : 2-amino pyridine
Compound II : 3-amino pyridine
Compound III : 3-methyl pyridine
Compound IV : 3-amido pyridine

EXPERIMENTAL

Spectroscopically pure iron (Johnson & Matthey, England) was used throughout the present work. Specimens of 1.6 cm length and 0.42 cm diameter were cut and smoothed on a polishing machine. The electrode was fixed to pyrex glass tubing with araldite. Electrical contact was achieved through thick copper wires soldered to the end of the rod, not exposed to the solution. The surface treatment included polishing with finest grade emery paper, washing with bidistilled water and degreasing with acetone.

All chemicals used were of analytical grade and used without further purification.

The test electrode half cell was made of pyrex glass and had inlet and outlet for nitrogen. Before starting polarization, the electrode was immersed in the electrolyte. Temperature was 25±1°. Purified nitrogen gas was bubbled through the solution for 30 minutes (2-3 bubble per second) before immersion of the electrode and continued during the measurements. The potential of iron electrode relative to a saturated calomel electrode (S.C.E.) was traced using a Wenking potentiometer (Type C.G- 822). The potential-time curve recording started before the start of polarization and continued till the steady state potential was reached; then the external current was applied to the cell. Details of the experimental procedure, electrolytic cell and electrical circuit are fully described elsewhere [9].

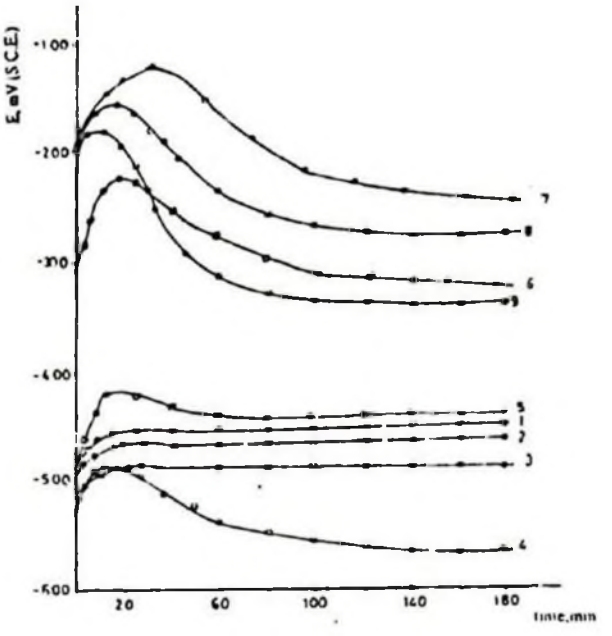


Fig 1 Potential - Time Curves of Iron
Media: Different Concentrations of Tartaric Acid
1) 1 M; 2) $1x10^{-1}$ M; 3) $1x10^{-2}$ M; 4) $1x10^{-3}$ M;
5) $5x10^{-4}$ M; 6) $2x10^{-4}$ M; 7) $1x10^{-4}$ M;
8) $1x10^{-5}$ M; 9) $1x10^{-6}$ M.

RESULTS AND DISCUSSION

Effect of Acid Concentration

The variation of potential of Fe electrode with time in deaerated tartaric acid solutions of varying concentrations (10^{-6} -

1M) is presented in Figure 1. This Figure indicates:

(i) Upon immersion of the electrode in tartaric acid solutions, the measured potential starts from negative values and approaches a steady state value.

(ii) At acid concentrations higher than 10^{-3} M, there is a slight shift of the potential towards less negative direction before approaching the steady state values.

(iii) In acid concentration range 10^{-6} - 10^{-4} M, the potential of the electrode shifts to noble values before reaching the steady state potential.

Practically all metals are covered with an air-formed pre-immersion oxide film. Though the potential of iron becomes noble after immersion in tartatic acid solutions, the pre-immersion oxide film is not sufficient to impart passivity.

In deaerated acid solutions, the most common cathodic reaction is the evolution of hydrogen (eq. 1):

$$2H + 2e \longrightarrow H_2 \qquad (1)$$

The electrons necessary for the reduction process are furnished from the ionization of iron atom entering the oxide phase and solution.

The Figure 2 shows the cathodic polarization curves of Fe electrode in deaerated tartaric acid solutions of

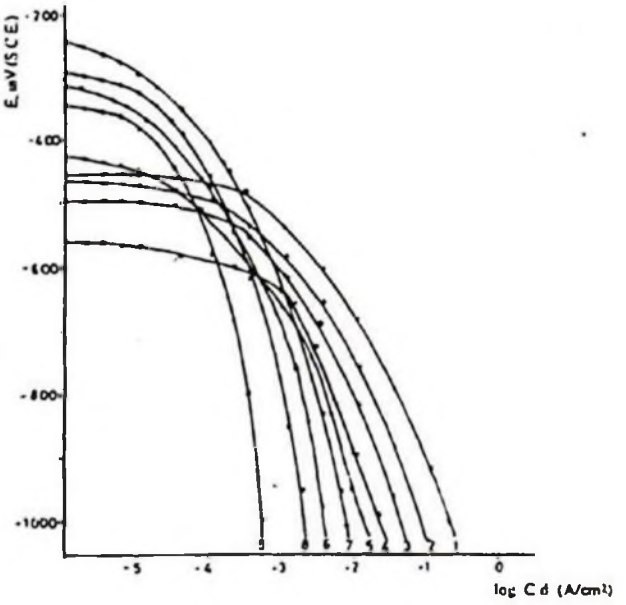


Fig 2 Cathodic Polarization Curves of Iron
Media: Different Concentrations of Tartaric Acid
1) 1 M; 2) $1x10^{-1}$ M; 3) $1x10^{-2}$ M; 4) $1x10^{-3}$ M; 5) $5x10^{-4}$ M; 6) $2x10^{-4}$ M; 7) $1x10^{-4}$ M; 8) $1x10^{-5}$ M; 9) $1x10^{-6}$ M.

concentrations ranging between 1 and 1 x 10^{-6} M at 25°C. The corrosion current density (i_{corr}) was determined from the intersection of the extrapolated cathodic Tafel line (linear part) with the corrosion potential (E_{corr}).

The corrosion rate (R_{corr}) in millimeter per year (MPY) can be calculated by the following equation [10].

$$R_{corr} = \frac{0.13\ I_{corr}\ W_e}{d} \qquad \ldots (2)$$

where I_{corr} is the corrosion current density in microamperes per square centimeter. W_e is the equivalent weight of the corroding species (W_e of Fe = 55.847) and d is the density (d of Fe = 7.86 $gm.cm^{-3}$).

The electrochemical parameters were computed from the cathodic polarization curves of Fe electrode in tartaric acid of varying concentrations and represented in Table 1.

Table 1

Effect of Tartaric acid Concentration on Corrosion Parameters

(E_{corr}) Corrosion Potential *vs* SCE (mV);
(i_{corr}) Corrosion Current Density in $(A/cm^2)x10^{-4}$;
(R_{corr}) Corrosion Rate (MPY) .

Acid, M	E_{corr}	i_{corr}	R_{corr}
1.00	-450	8.912	823.468
1×10^{-1}	-465	5.623	519.565
1×10^{-2}	-495	3.162	292.168
1×10^{-3}	-565	2.512	232.108
5×10^{-4}	-440	1.362	125.848
2×10^{-4}	-310	1.202	111.064
1×10^{-4}	-230	1.000	92.400
1×10^{-5}	-280	0.707	65.327
1×10^{-6}	-340	0.398	36.775

The table shows that corrosion potential decreases linearly with log C till 10^{-3} M acid; at much lower concentrations, it increases till 10^{-4} and decreases again at still lower concentrations. It is clear that, the curve has generally the same features with a minimum potential at 10^{-3} M acid concentration. The above relationship gave straight lines with different slopes in the two concentration regions according to Bracher equations [11].

$$E_{corr} = a \pm b \log C \quad \ldots (3)$$

where a and b are constants depending upon the type of electrode and electrolyte.

An inspection of the data given in Table 1 reveals that the corrosion current density (i_{corr}) and consequently the corrosion rate (R) increases with the acid concentration, indicating the acceleration of corrosion process inspite of the shift of the corrosion potential into the positive direction.

The shift of the corrosion potential in the noble direction and the simultaneous increase of the corrosion rate [12,13] with increase of acid concentration may be ascribed to either / both of the following reasons :

(a) $-d[H^+]/dt = K[H^+] \exp(\alpha FE/RT)$ ....(4)

where K is constant, α is the transfer coefficient, F is the Faraday constant, E is the electrode potential, R is the gas constant and T is the absolute temperature. The rate corresponding to a certain potential (provided that α is constant) should increase with the increase of H^+, so that the E-I curves [14] of the cathodic reaction move on the current axis towards high currents.

b) The local cathodic polarization curve shifts in the positive direction by an amount given by the Nernst equation (assuming that the slope of the anodic E-I curves is not changed).

Effect of Addition of Pyridine Derivatives on the Dissolution of Fe in 0.001 M Tartaric Acid

Fig. 3 represents the effect of different concentrations of 2-amino pyridine on the potential-time curves of Fe in 10^{-3} M tartaric acid. Similar curves were obtained using other compounds (not shown). The curves reveal that, the potential of Fe electrode shifts first to positive values and then decreased gradually till steady-state values were reached.

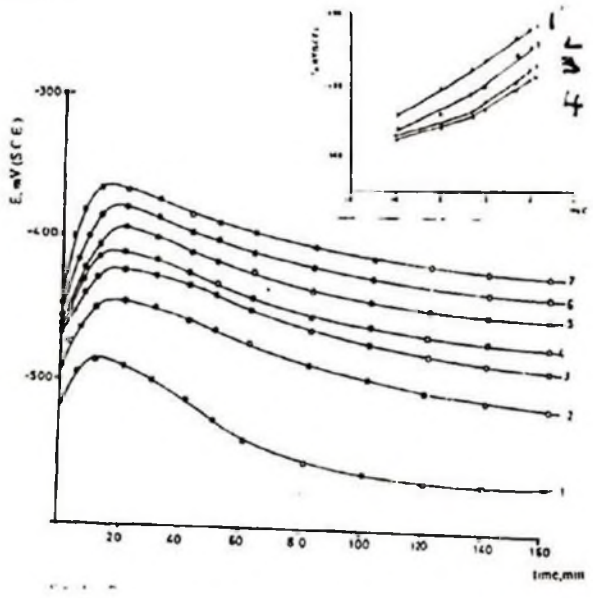


Fig 3 Potential - Time Curves of Iron
Media: $1x10^{-3}$ M of Tartaric Acid Containing different Concentrations of 2-amino pyridine
1) 0 M; 2) $1x10^{-5}$ M; 3) $1x10^{-4}$ M; 4) $5x10^{-4}$ M; 5) $1x10^{-3}$ M; 6) $5x10^{-3}$ M; 7) $1x10^{-2}$ M;
Inset: Steady State Potential as a Function of Conc. of Different Inhibitors
1) 2-amino pyridine 2) 3-amino pyridine; 3) 3-methyl pyridine; and 4) 3-amido pyridine.

The relationship between the steady state potential and the logarithm of the molar concentration of the inhibitor compounds is shown in the inset. The steady state potential is seen to shift toward positive

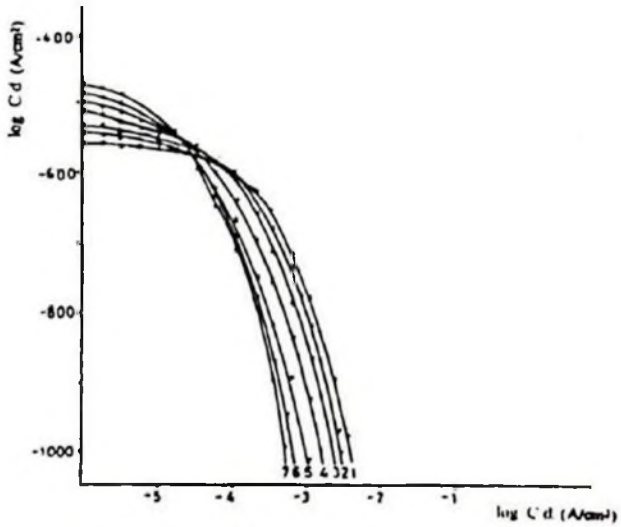


Fig 6 Cathodic polarization curves of Fe in a 1×10^{-3} M tartaric acid solution containing different concentrations of compound II

Fig 4 Cathodic Polarization Curves of Iron
Media: 1x10Pt-3Pt M Tartaric acid Containing Different Concentrations of 3-amino pyridine
1) 0 M; 2) $1x10^{-5}$ M; 3) $1x10^{-4}$ M; 4) $5x10^{-4}$ M; 5) $1x10^{-3}$ M; 6) $5x10^{-3}$ M; 7) $1x10^{-2}$ M;

direction as the additives concentration is increased. This indicates that these compounds inhibit the corrosion of Fe in tartaric acid.

The effect of increasing concentrations of 3-amino pyridine on the cathodic polarization curves of iron electrode in 1 x 10^{-3} M tartaric acid solution is shown in Fig 4. The polarization curves in presence of the other three derivatives are similar.

The inhibition efficiency (I.E.) was calculated from :

$$I.E. = 100 \left[1 - \frac{R_{corr\,(add)}}{R_{corr\,(free)}} \right] \quad \ldots (5)$$

where $R_{corr.(add)}$ and $R_{corr.(free)}$ are the corrosion rates in presence and absence of the inhibitors, respectively.

Table 2

Effect of Inhibitor Concentration on the Corrosion Parameters

Corrosion potential vs SCE (E_{corr}) in mV, Corrosion Current Density (I_{corr}) in $A.cm^{-2} \times 10^{-4}$, Corrosion Rate (R_{corr}) in MPY, Inhibition Efficiency (I.E.) and Surface Coverage (θ) for dissolution of iron electrode.

Medium 1×10^{-3} M tartaric acid with different Concentration of Inhibitors

Inhib. Conc.	E_{corr}	I_{corr}	R_{corr}	I.E.	θ
Inhibitor: 2-amino pyridine					
0.00 M	-565	2.512	232.108		
1×10^{-5} M	-508	1.000	92.400	60.19	0.6019
1×10^{-4} M	-490	0.891	82.328	64.53	0.6453
5×10^{-4} M	-468	0.501	46.292	80.05	0.8005
1×10^{-3} M	-455	0.398	36.775	84.15	0.8415
5×10^{-3} M	-430	0.316	29.198	87.42	0.8742
1×10^{-2} M	-420	0.239	22.084	90.48	0.9042
Inhibitor: 3-amino pyridine					
0.00 M	-565	2.512	232.108		
1×10^{-5} M	-530	1.202	111.064	52.14	0.5214
1×10^{-4} M	-510	0.794	83.365	68.39	0.6839
5×10^{-4} M	-495	0.631	58.304	74.88	0.7488
1×10^{-3} M	-485	0.562	51.928	77.62	0.7762
5×10^{-2} M	-450	0.355	32.802	85.86	0.8586
$+1 \times 10^{-2}$ M	-435	0.275	25.410	89.05	0.8905
Inhibitor: 3-methyl pyridine					
0.00 M	-565	2.512	232.108		
1×10^{-5} M	-535	1.380	127.547	45.06	0.4506
1×10^{-4} M	-525	1.023	94.525	59.27	0.5927
5×10^{-4} M	-515	0.631	58.304	74.88	0.7488
1×10^{-3} M	-505	0.501	46.292	8.05	0.8005
5×10^{-3} M	-485	0.398	36.775	84.16	0.8416
1×10^{-2} M	-468	0.316	29.198	87.42	0.8742
Inhibitor: 3-amido pyridine					
0.00 M	-565	2.512	232.108		
1×10^{-5} M	-538	1.318	121.780	47.53	0.4753
1×10^{-4} M	-528	1.047	96.792	58.32	0.5832
5×10^{-4} M	-520	0.794	73.365	68.39	0.6839
1×10^{-3} M	-510	0.562	51.930	77.63	0.7763
1×10^{-3} M	-490	0.446	41.210	82.90	0.8590
1×10^{-2} M	-482	0.354	32.704	85.90	0.8590

Table 2 shows the effect of pyridine compounds on the corrosion potential (E_{corr}), corrosion rate (R), inhibition efficiency (I.E.) and surface coverage (θ).

The above results show that the pyridine derivatives act as inhibitors. (Increasing the concentration of the pyridine compounds causes decrease of i_{corr} and corrosion rate R_{corr} and thus increase the value of inhibition efficiency I.E.).

The dissolution of Fe in acidic solution may be described as follows [13].

$$Fe + OH \rightleftharpoons (FeOH)_{ads} + e \quad \ldots (6)$$

$$(FeOH)_{ads} \longrightarrow (FeOH)^{\bullet}_{ads} + e \quad \ldots (7)$$

$$(FeOH)^{\bullet}_{ads} \longrightarrow Fe^{2\bullet} + OH \quad \ldots (8)$$

where step (6) is in quasi-equilibrium, step (7) is the rate determining step of the overall process, and step (8) is fast. The introduction of species which could simultaneously trap the $(FeOH)_{ads}$ from the surface (e.g. pyridine derivatives), and consume the surface sites (by an appropriate adsorption mechanism) will inhibit the general corrosion of the metal.

Pyridine derivatives are basic compounds. In acidic media like the present, they cannot remain in solutions as free bases; it is assumed that they exist initially in cationic form at the metal/solution interface. After corrosion has commenced, the inhibitor cations can become attached to anodic sites. It is also possible that the alkalinity produced at cathodic sites favour the free base molecular form which can then be generally adsorbed on the metal surface. A similar mechanism has been proposed by Kaesche and Hackerman [15] for inhibition of iron in hydrochloric acid by organic amines.

The steady state potential values as a function of different concentrations of the inhibitors (cf. the inset fig in Fig 3) shows the order of inhibitor action as 2-amino pyridine > 3-amino pyridine > 3-methyl pyridine > 3-amido pyridine.

This sequence can be explained on the basis of the electron density on the nitrogen atom in the pyridine ring. This varies according to the nature and position of the substituents in the ring. The electron density affects the chemisorption of the compound on the metal surface (with the formation of a metal nitrogen coordination bond). In 2-amino pyridine and 3-amino pyridine, NH_2 group has (+R), CH_3 group in 3-methyl pyridine has (+I), while $CONH_2$ group in 3-amido pyridine has (-R) effect. So, the lone pair of electrons on nitrogen atom of the ring are more localized in the order: 2-amino pyridine > 3-amino pyridine > 3-methyl pyridine > 3-amido pyridine. The higher inhibiting effect of 2 amino pyridine than 3-amino pyridine is attributed to the position of NH_2 group in the ring. The ring in 2-amino pyridine is more activated than in 3-amino pyridine due the presence of amino group in 2-position which facilitates the donation of electron to the N-atom of the ring than in 3-position.

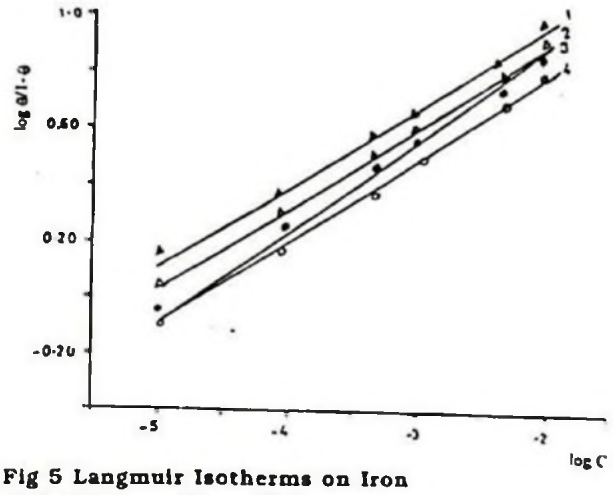


Fig 5 Langmuir Isotherms on Iron
1) 2-amino pyridine 2) 3-amino pyridine;
3) 3-methyl pyridine; and 4) 3-amido pyridine.

Adsorption Behaviour

The inhibitive efficiency of pyridine compounds is determined by their adsorbability on the surface of the corroding metal. It is assumed that a part of the metal surface (θ) is covered by inhibitor as a result of adsorption and thus becomes inactive. The degree of surface coverage θ can be calculated by dividing the value of I.E. in equation (5) by 100 (I.E./100).

Fig.5 shows a plot of θ/(1-θ) *vs* C on a double logarithmic scale. The inhibitors used show a reasonable linear relationship between the two variables, but the gradient of the plots deviates from unity, in contrast to findings of Langmuir [16] and Hoar [17]. This deviation could be explained in terms of mutual attraction and / or repulsion of the adsorbed species to each other - a fact which was ignored during derivation of Langmuir isotherm [16].

REFERENCES

1. M.A. El Moris, M.M. Ghoneim, F. M. Issa, E.M. Mabrouk, *Surf. and Coat. Technol.*, **31** (1987) 389.
2. H.H. Uhlig, *Corrosion and Corrosion Control*, 2nd Edn. **John Wiley, Newyork** (1963).
3. V.K. Gouda, S.M. Abd Elwahab, E.M. Ibrahim, *Corros. Sci.*, **20** (1980) 1091.
4. P.N.S. Yadav, R.W. Adhwani, *Bull. Electrochemistry* **9** (1993) 62.
5. M. Abdallah, H.E. Megahed, *Monatshefte fur Chemie*, **126** (1995) 519-527.
6. A.Y. El Etre and M. Abdallah, *Bull. Electrochemistry* **10(11-12)** (1994) 471-476.
7. M. Abdallah and A.I. Mead, *Annali Di Chimica (Rome)*, **83** (1993) 423-430.
8. M. Abdallah, *Annali Di Chimica (Rome)*, **84** (1994) 529.
9. I. Ammar, S.Darwish, M. Etman, *Electrochem. Acta.*, **12** (1967) 485.
10. A.A. Abd El Fattah, E.M. Mabrouk, R.M. Abd El Gulil, M.M. Ghoneim, *Bull. Soc. Chim. Fr.*, **127** (1991) 48-53.
11. D.M. Brasher, *Nature, London*, **193** (1963) 868.
12. H.E. Megahed, Ph.D. Thesis, **Zagazig Univ. Benha Branch, Benha**, Egypt (1988).
13. LI Antropov, *Theoretical Electrochemistry*" **Mir Publisher, Moscow** (1973) 503.
14. R.F. Steigrewald, *Corrosion* **14** (1968) 1.
15. H. Kaesche, N. Hackerman, *J. Electrochem. Soc.*, **105** (1958) 191.
16. I. Langmuir, *J. Am. Chem. Soc.*, **38** (1916) 222.
17. T.P. Hoar, R.V. Halliday, *J. Appl. Chem. (London)*, **3** (1952) 505.